Kinematics and geometry of active detachment faulting beneath the Trans-Atlantic Geotraverse (TAG) hydrothermal field on the Mid-Atlantic Ridge

Brian J. deMartin* Massachusetts Institute of Technology–Woods Hole Oceanographic Institution Joint Program in Oceanography, Cambridge, Massachusetts 02139, USA

Robert A. Sohn
Juan Pablo Canales
Susan E. Humphris
Woods Hole Oceanographic Institution, Woods Hole, Massachusetts 02543, USA

ABSTRACT

Newly acquired seismic refraction and microearthquake data from the Trans-Atlantic Geotraverse (TAG) segment of the Mid-Atlantic Ridge at 26°N reveal for the first time the geometry and seismic character of an active oceanic detachment fault. Hypocenters from 19,232 microearthquakes observed during an eight month ocean bottom seismometer deployment form an ~15-km-long, dome-shaped fault surface that penetrates to depths >7 km below the seafloor on a steeply dipping (~70°) interface. A tomographic model of compressional-wave velocities demonstrates that lower crustal rocks are being exhumed in the detachment footwall, which appears to roll over to a shallow dip of 20° ± 5° and become aseismic at a depth of ~3 km. Outboard of the detachment the exhumed lithosphere is deformed by ridge-parallel, antithetical normal faulting. Our results suggest that hydrothermal fluids at the TAG field exploit the detachment fault to extract heat from a region near the crust-mantle interface over long periods of time.

Keywords: detachment faults, hydrothermal vents, Mid-Atlantic ridge, tectonics, earthquakes, seismic profiles.

INTRODUCTION

The Trans-Atlantic Geotraverse (TAG) segment of the Mid-Atlantic Ridge is notable for being the site of one of the largest and best-studied hydrothermal fields on the deep seafloor (Rona et al., 1993, 1986; Scott et al., 1974). Hydrothermal venting has been active at TAG for the past ~140 k.y. (Lalou et al., 1995), and has generated several large mineral deposits within an ~5 × 5 km area on the eastern side of the Mid-Atlantic Ridge axial valley at 26°08′N (Fig. 1). High-temperature activity is currently focused at the active TAG mound (Humphris and Tivey, 2000; Kleinrock and Humphris, 1996), a massive sulfide deposit ~200 m diameter and ~50 m tall containing ~3.9 ×10^9 kg of sulfides (Humphris et al., 1995) and discharging fluids having temperatures in excess of 360 °C (Campbell et al., 1988; Chiba et al., 2001; Parker and von Damm, 2005).

The geological conditions and processes that allow for long-lived, focused hydrothermal discharge and the formation of large mineral deposits in the TAG region have been the topic of considerable speculation. Early research focused primarily on heat extraction from a mid-crustal melt reservoir at the axis (Kong et al., 1992), possibly via circulation through listric faults (Temple et al., 1979; Thompson et al., 1985). Later scenarios favored shallow convection from a local heat source directly beneath the hydrothermal field (Rona et al., 1993; Zonenshain et al., 1989) or removal of heat through a broad cracking front penetrating downward into the lower crust (Wilcock and Delaney, 1996). The bathymetric salient east of the hydrothermal field has been interpreted as an inside corner high (Tucholke and Lin, 1994), and gabbro and diabase outcrops have been observed on the eastern rift valley wall (Reves-Sohn et al., 2004; Zonenshain et al., 1989). Near-bottom magnetics data have revealed a zone of reduced magnetization on the eastern valley wall (Tivey et al., 2003), interpreted to result from crustal thinning by long-lived extension on a normal fault. These data led to the hypothesis that the hydrothermal field is situated on the hanging wall of an active detachment fault, emphasizing the role of tectonic, rather than volcanic, processes for maintaining long-lived hydrothermal circulation at the TAG hydrothermal field (Tivey et al., 2003).

SEISMIC OBSERVATIONS

We conducted an ocean bottom seismometer (OBS) experiment to better define the geological processes that give rise to long-lived hydrothermal circulation at the TAG field. We recorded continuous microearthquake data for eight months using a 7 × 7 km network of 13 short-period 4-component OBSs (Fig. 1), and complemented these observations with a seismic refraction survey using the R/V *Maurice Ewing* airgun array (8760 in^3, 350 m shot spacing). Our main objectives were to use the microearthquake data to determine the mechanics of faulting, and to use the refraction data to define the crustal architecture of the TAG segment.

We detected and located 19,232 microearthquakes (~80 events/day, average rate) along an ~30 km stretch of the ridge axis with local magnitudes $1 \le M_L \le 4$ during our OBS deployment. Hypocenter estimates were made via stochastic descent on a three-dimensional grid using residuals from compressional and shear (*P* and *S*) phase arrivals picked from the seismometer records (see the GSA Data Repository[1]). Predicted arrival times were estimated using a bathymetry conforming, depth-averaged velocity model derived from the refraction survey (Fig. 2B, inset). Seismic velocities below the depth limit of the refraction survey were determined using typical Mid-Atlantic Ridge values (Hooft et al., 2000) with a fixed depth below the seafloor (6 km) for the crust-mantle interface. Mean hypocenter accuracies (95% confidence level) are ±1.0, 0.9, and 1.1 km in the N-S, E-W, and vertical directions, respectively (a hypocentral catalogue with uncertainties and residuals for each earthquake is available in the GSA Data Repository).

Two distinct zones of seismic activity are evident in the hypocentral records; one set of events forms an arc that wraps around the bulge on the east side of the axial valley, and a second set strikes parallel to the ridge beneath the eastern valley wall (Fig. 1A). The events along the arc occur on a steep (~70°), west-dipping fault that extends at least 7 km below the seafloor (Fig. 2A). Composite focal mechanisms (GSA Data Repository) obtained by combining first

*Current address: Brown University, 324 Brook Street, Box 1846, Providence, Rhode Island 02912, USA.

[1]GSA Data Repository item 2007183, Figure DR1 (earthquake waveforms and picks), Table DR1 (hypocenter catalog), and Figure DR2 (active-source seismic record), is available online at www.geosociety.org/pubs/ft2007.htm, or on request from editing@geosociety.org or Documents Secretary, GSA, P.O. Box 9140, Boulder, CO 80301, USA.

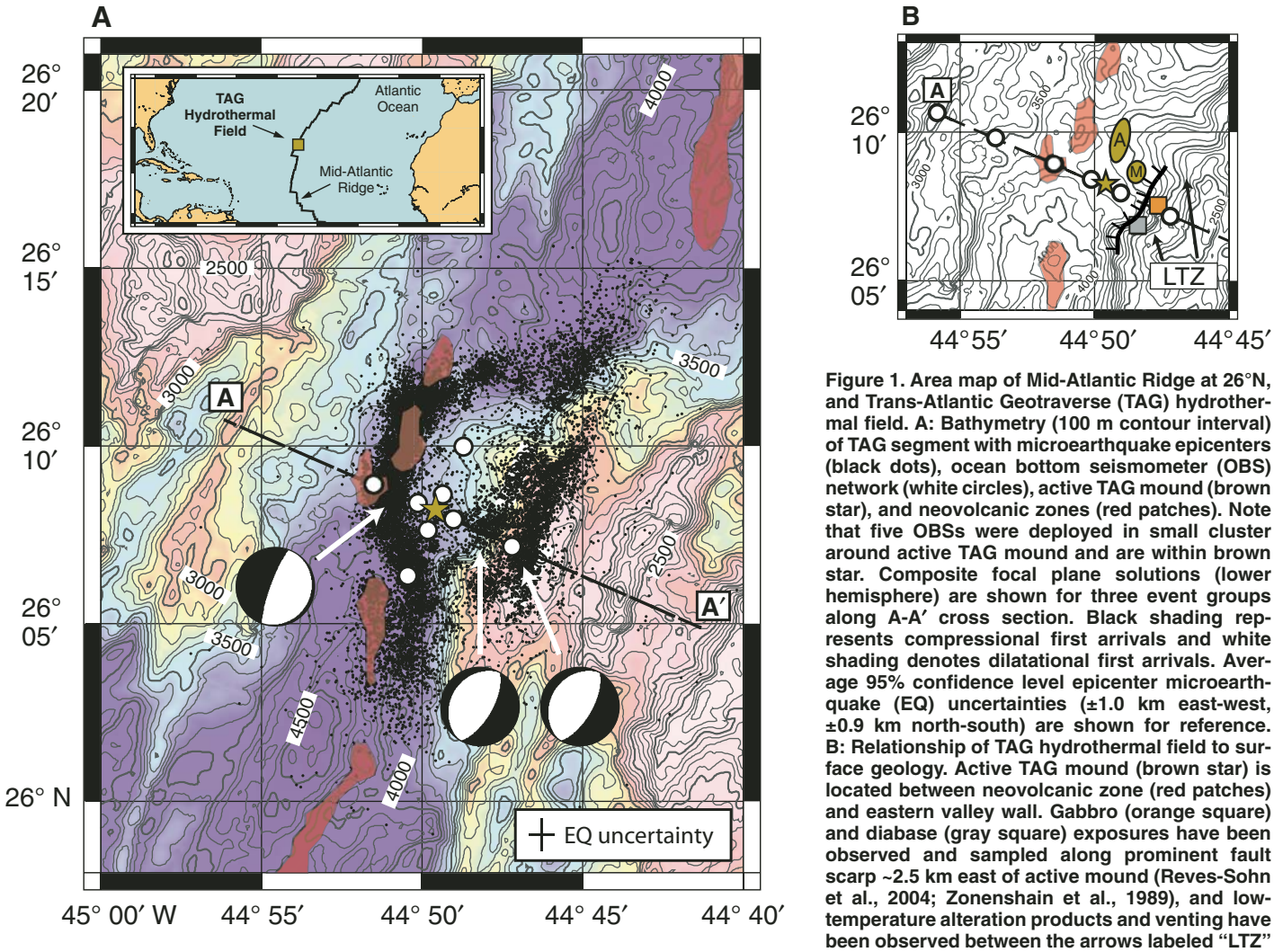

Figure 1. Area map of Mid-Atlantic Ridge at 26°N, and Trans-Atlantic Geotraverse (TAG) hydrothermal field. A: Bathymetry (100 m contour interval) of TAG segment with microearthquake epicenters (black dots), ocean bottom seismometer (OBS) network (white circles), active TAG mound (brown star), and neovolcanic zones (red patches). Note that five OBSs were deployed in small cluster around active TAG mound and are within brown star. Composite focal plane solutions (lower hemisphere) are shown for three event groups along A-A′ cross section. Black shading represents compressional first arrivals and white shading denotes dilatational first arrivals. Average 95% confidence level epicenter microearthquake (EQ) uncertainties (±1.0 km east-west, ±0.9 km north-south) are shown for reference. B: Relationship of TAG hydrothermal field to surface geology. Active TAG mound (brown star) is located between neovolcanic zone (red patches) and eastern valley wall. Gabbro (orange square) and diabase (gray square) exposures have been observed and sampled along prominent fault scarp ~2.5 km east of active mound (Reves-Sohn et al., 2004; Zonenshain et al., 1989), and low-temperature alteration products and venting have been observed between the arrows labeled "LTZ" for low-temperature zone (Rona et al., 1993). Relict high-temperature zones (brown patches; M—Mir zone, A—Alvin zone) are located northeast of active TAG mound. OBSs (white circles) used for seismic refraction velocity inversion are shown along cross section.

arrival polarities from ~300 individual events are consistent with normal faulting along the hypocentral trend (dip 80°). Seismic activity on this fault decreased dramatically at depths <~3 km (detection threshold of $M_L \geq 1$). The ridge-parallel microearthquakes beneath the eastern valley wall form two spatially distinct clusters at depths of ~2–5 km below the seafloor. The spatial association of these events with discrete fault planes is somewhat ambiguous, but composite focal mechanisms for both clusters are consistent with antithetic normal faulting on planes dipping eastward (away from the spreading axis) at 65° (Fig. 1A).

We inverted *P*-wave first arrival traveltimes using the method of Korenaga et al. (2000) to generate a tomographic model of seismic velocities across the ridge axis (Fig. 2; GSA Data Repository). We find that crustal structure is highly asymmetric across the axial valley. The western side of the axial valley has a seismic structure similar to other volcanically constructed Mid-Atlantic Ridge segments (e.g., Hooft et al., 2000; White et al., 1992), but the eastern flank is underlain by a large, high-velocity anomaly. Seismic velocities at depths below 1 km on the eastern flank exceed 6.5 km/s (compared to 4.5 km/s beneath the neovolcanic zone), indicating the presence of lower crustal and/or serpentinized upper mantle rocks at anomalously shallow depths. The velocity anomaly dips toward the spreading axis at an angle of 20° ± 5°, passes under the active TAG mound at a depth of ~1 km (Fig. 2A), and intersects the hypocenter trend of the west-dipping fault plane at a depth of ~3 km. Although our cross-axis tomography model is limited to the upper ~2.5 km of the crust, additional tomography models obtained along the axial valley (Canales et al., 2005) do not contain any low-velocity zones indicative of crustal melts at the TAG segment, in contrast to the Kong et al. (1992) seismological study of this same area.

DISCUSSION

Our results provide important new constraints for the geometry of faulting and the crustal architecture in the TAG region. We find that lithospheric extension on the east side of the axial valley is being accommodated on a curved normal fault with a steep (~70°) dip over the depth interval of ~3–7 km below the seafloor. We did not detect significant levels of seismic activity on the fault at depths <~3 km, but the shallow fault geometry is delimited by our tomographic velocity model. Seismic (*P*-wave) velocities on the east side of the axial valley exceed 6.5 km/s at depths as shallow as ~1 km beneath the seafloor, and indicate that the fault exhumes lower crustal rocks on a low-angle interface dipping at ~20° toward the spreading axis, consistent with geological observations at other detachment faults (e.g., Dick et al., 1981; Cann et al., 1997; Smith et al., 2006). The inferred footwall–hanging-wall interface intercepts the west-dipping normal fault just above the depth where

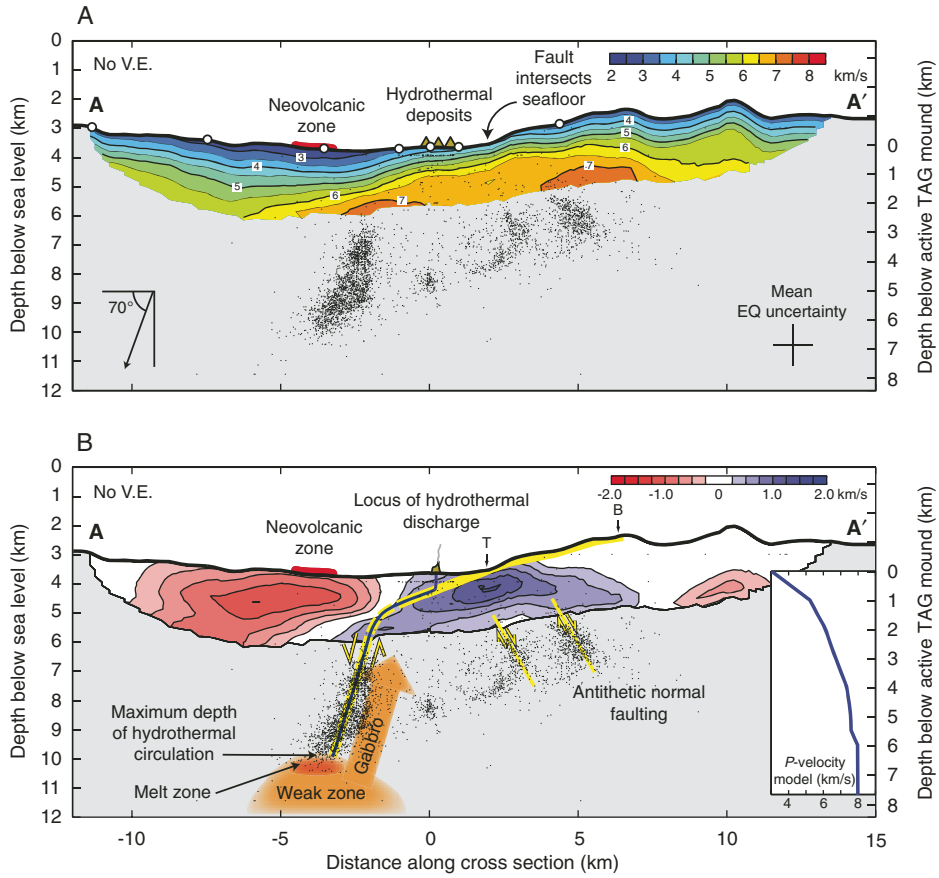

Figure 2. Depth sections (no vertical exaggeration) across axial valley on A-A′ (from Fig. 1). A: *P*-wave velocity model and hypocenters from events within 1 km of cross section. Tomographic model uncertainties are typically <0.1 km/s, but can be as large as 0.2 km/s at eastern end of model. Position of neovolcanic zone, hydrothermal deposits, fault termination, and ocean bottom seismometers (OBSs) (white circles) used for velocity inversion along cross section are also shown. Average 95% confidence level hypocentral uncertainties (projected along cross section) are shown for reference (depth uncertainty is ±1.1 km). B: Schematic model of crustal accretion, deformation, and hydrothermal circulation at Trans-Atlantic Geotraverse (TAG) with hypocenters and *P*-wave velocity model used to define earthquake hypocenters. Tomographic results are shown as perturbations against one-dimensional average model, as opposed to absolute velocities. Extension on east side of spreading axis is accommodated on dome-shaped detachment fault and on two distinct planes of antithetic normal faulting (yellow lines). New lithosphere is formed by exhuming lower crustal material on fault footwall. Detachment fault is exposed at seafloor from termination (T) to breakaway (B) as identified from magnetic data (Tivey et al., 2003). Long-lived, high-temperature hydrothermal circulation at TAG hydrothermal field requires magmatic heat source (e.g., Cann and Strens, 1982; Humphris and Cann, 2000), but our seismic velocity model and earthquake hypocenters effectively preclude presence of crustal magma chamber. This suggests that there must be deep melt reservoir beneath neovolcanic zone, which may also root high-angle normal fault. Gabbros crystallizing from this reservoir would then be accreted onto footwall (orange arrow) during extension. Hydrothermal fluids may flow through hanging wall at shallow depths, but they must be focused on detachment deeper in crust, and they must penetrate to depths of ≥7 km to extract high-temperature heat from base of fault.

it becomes aseismic (Fig. 2B), suggesting that the change in seismic behavior is associated with rollover to a low-angle geometry. The transition to aseismic slip on a low-angle plane is consistent with rolling-hinge models (e.g., Buck, 1988) and constraints from faulting mechanics. The relative lack of seismicity along shallow-dipping normal faults is also a well-documented characteristic of continental detachments (Collettini and Sibson, 2001; Jackson and White, 1989) and global seismicity compilations (e.g., Wernicke, 1995).

The deeply penetrating normal fault curves around the eastern axial valley wall, isolating an ~15-km-long, dome-shaped lens of material from the rest of the spreading axis. Near-bottom magnetics data show that the crust has been thinned by ~3.9 km of horizontal extension (Tivey et al., 2003), and place the fault termination ~2.5 km east of the active TAG mound, in roughly the same place where gabbro and diabase outcrops have been observed and/or sampled on the seafloor (Reves-Sohn et al., 2004; Zonenshain et al., 1989) (Fig. 1B). The low-angle fault geometry inferred from our seismic velocity model is required to reconcile our microearthquake patterns with the magnetics data, because any surface connecting the fault termination with the arc of seismicity will necessarily have a dip ≤30° (Fig. 2B). A low-angle fault geometry in the shallow crust is also required to reconcile the footwall vertical relief (~1.5 km) with the horizontal extension required by the magnetics data (~3.9 km). Alternative models without significant rollover of the west-dipping normal fault are effectively precluded by dive observations (Karson and Rona, 1990; Zonenshain et al., 1989) and high-resolution sidescan sonar images (Kleinrock and Humphris, 1996) of the axial valley; these images provide no evidence of large-offset fault scarps or hydrothermal discharge within the neovolcanic zone. We cannot provide a plausible faulting model that satisfies the combination of our seismic data, the magnetics data, the sidescan sonar data, the bathymetric data, and the dive observations from the TAG region without invoking a rollover to a low-angle geometry at shallow depths.

We estimate a total fault rollover of ~50° (i.e., 70° to 20°) when all the relevant information is considered. This amount of rollover is consistent with paleomagnetic rotations measured at the Fifteen-Twenty and Atlantis massif oceanic core complexes (Blackman et al., 2006; Garcés and Gee, 2007), as well as rotations deduced for some continental core complexes (e.g., Manatschal et al., 2001). Highly rotated crustal blocks, however, have not been observed in the footwall east of TAG (e.g., Karson and Rona, 1990; Zonenshain et al., 1989), which is consistent with the fact that the detachment fault has only been active long enough (~350 k.y.) to exhume ~1.5 km of largely unrotated upper crust. Although the footwall exhibits a dome-shaped morphology, it lacks the surface corrugations associated with more advanced stages of core complex evolution (e.g., Smith et al., 2006), also supporting a young age for the detachment.

We conclude that the TAG hydrothermal field is located on the hanging wall of an active, but young, oceanic detachment, and we use the kinematic and geometric data provided by our seismic study to develop a schematic model of lithospheric extension, crustal accretion, and hydrothermal circulation (Fig. 2B). We find no evidence for any crustal melt reservoirs, and our results suggest that hydrothermal fluids must penetrate to >7 km depth below the seafloor to extract heat from a source large enough (e.g., Humphris and Cann, 2000) to drive long-term, high-temperature hydrothermal convec-

tion. Long-term hydrothermal circulation and the generation of large mineral deposits at the TAG field appear to be direct consequences of the detachment faulting process, which allows hydrothermal fluids to tap heat from a deep melt reservoir near the crust-mantle interface.

ACKNOWLEDGMENTS

We thank Joe Cann, Hans Schouten, Mark Behn, and Jeff Gee for helpful discussions, Jeff Karson, Donna Blackman, Jon Spencer, and an anonymous referee for helpful reviews, the Woods Hole Oceanographic Institution and Lamont-Doherty Earth Observatory ocean bottom seismography instrument groups for technical support, and the ship's crews of the R/Vs *Atlantis*, *Maurice Ewing*, and *Knorr* for their efforts at sea. This work was supported by National Science Foundation grant OCE-0137329.

REFERENCES CITED

Blackman, D.K., Ildefonse, B., John, B.E., Ohara, Y., Miller, D.J., MacLeod, C.J., and Expedition 304/305 Scientists, 2006, Proceedings of the Integrated Ocean Drilling Program, Volume 304/305: College Station, Texas, Integrated Ocean Drilling Program, doi: 10.2204/iodp.proc.304305.2006.

Buck, R.W., 1988, Flexural rotation of normal faults: Tectonics, v. 7, p. 959–973.

Campbell, A.C., Palmer, M.R., Klinkhammer, G.P., Bowers, T.S., Edmond, J.M., Lawrence, J.R., Casey, J.F., Thompson, G., Humphris, S., Rona, P.A., and Karson, J.A., 1988, Chemistry of hot springs on the Mid-Atlantic Ridge: Nature, v. 335, p. 514–519, doi: 10.1038/335514a0.

Canales, J.P., Reves-Sohn, R., and Humphris, S., 2005, Tectonism and long-lived hydrothermal systems: Seismic constraints from the TAG Segment, Mid-Atlantic Ridge 26°N: American Geophysical Union, Fall Meeting 2005, abs. OS33A–1467.

Cann, J.R., and Strens, M.R., 1982, Black smokers fuelled by freezing magma: Nature, v. 298, p. 147–149, doi: 10.1038/298147a0.

Cann, J.R., Blackman, D.K., Smith, D.K., McAllister, E., Janssen, B., Mello, S., Avgarinos, E., Pascoe, A.R., and Escartín, J., 1997, Corrugated slip surfaces formed at ridge-transform intersections on the Mid-Atlantic Ridge: Nature, v. 385, p. 329–332.

Chiba, H., Masuda, H., Lee, S.Y., and Fujioka, K., 2001, Chemistry of hydrothermal fluids at the TAG active mound, MAR 26 degrees N, in 1998: Geophysical Research Letters, v. 28, p. 2919–2922, doi: 10.1029/2000GL012645.

Collettini, C., and Sibson, R.H., 2001, Normal faults, normal friction?: Geology, v. 29, p. 927–930, doi: 10.1130/0091–7613(2001)029<0927:NFNF>2.0.CO;2.

Dick, H.J.B., Thompson, W.B., and Bryan, W.B., 1981, Low angle faulting and steady-state emplacement of plutonic rocks at ridge-transform intersections: Eos (Transactions, American Geophysical Union), v. 62, p. 406.

Garcés, M.A., and Gee, J.S., 2007, Paleomagnetic evidence of large footwall rotations associated with low-angle faults at the Mid-Atlantic Ridge: Geology, v. 35, p. 279–282, doi: 10.1130/G23165A.1.

Hooft, E.E.E., Detrick, R.S., Toomey, D.R., Collins, J.A., and Lin, J., 2000, Crustal thickness and structure along three contrasting spreading segments of the Mid-Atlantic Ridge, 33.5°N–35°N: Journal of Geophysical Research, v. 105, p. 8205–8226, doi: 10.1029/1999JB900442.

Humphris, S.E., and Cann, J.R., 2000, Constraints on the energy and chemical balances of the modern TAG and ancient Cyprus seafloor sulfide deposits: Journal of Geophysical Research, v. 105, p. 28,477–28,488, doi: 10.1029/2000JB900289.

Humphris, S.E., and Tivey, M.K., 2000, A synthesis of geological and geochemical investigations of the TAG hydrothermal field; insights into fluid-flow and mixing processes in a hydrothermal system, *in* Dilek, Y., et al., eds., Ophiolites and ocean crust: New insights from field studies and the Ocean Drilling Program: Geological Society of America Special Paper 349, p. 213–235.

Humphris, S.E., and 24 others, 1995, The internal structure of an active sea-floor massive sulphide deposit: Nature, v. 377, p. 713–716, doi: 10.1038/377713a0.

Jackson, J.A., and White, N.J., 1989, Normal faulting in the upper continental crust: Observations from regions of active extension: Journal of Structural Geology, v. 11, p. 14–36.

Karson, J.A., and Rona, P.A., 1990, Block-tilting, transfer faults, and structural control of magmatic and hydrothermal processes in the TAG area, Mid-Atlantic Ridge 26°N; with Suppl. Data 90–21: Geological Society of America Bulletin, v. 102, p. 1635–1645, doi: 10.1130/0016–7606(1990)102<1635:BTTFAS>2.3.CO;2.

Kleinrock, M.C., and Humphris, S.E., 1996, Structural control on sea-floor hydrothermal activity at the TAG active mound: Nature, v. 382, p. 149–153, doi: 10.1038/382149a0.

Kong, L.S.L., Solomon, S.C., and Purdy, G.M., 1992, Microearthquake characteristics of a mid-ocean ridge along-axis high: Journal of Geophysical Research, v. 97, p. 1659–1685.

Korenaga, J., Holbrook, W.S., Kent, G.M., Kelemen, P.B., Detrick, R.S., Larsen, H.-C., Hopper, J.R., and Dahl-Jensen, T., 2000, Crustal structure of the southeast Greenland margin from joint refraction and reflection seismic tomography: Journal of Geophysical Research, v. 105, p. 21,591–21,614, doi: 10.1029/2000JB900188.

Lalou, C., Reyss, J.-L., Brichet, E., Rona, P.A., and Thompson, G., 1995, Hydrothermal activity on a 10^5-year scale at a slow-spreading ridge, TAG hydrothermal field, Mid-Atlantic Ridge 26°N: Journal of Geophysical Research, v. 100, p. 17,855–17,862, doi: 10.1029/95JB01858.

Manatschal, G., Froitzheim, N., Rubenach, M.J., and Turrin, B., 2001, The role of detachment faulting in the formation of an ocean-continent transition: Insights from the Iberia Abyssal Plain, *in* Wilson, R.C.L., et al., eds., Non-volcanic rifting of continental margins: Evidence from land and sea: Geological Society [London] Special Publication 187, p. 405–428.

Parker, C.M., and von Damm, K.L., 2005, Time series fluid compositions from the TAG Hydrothermal Mound, MAR: 1986–2004: American Geophysical Union, Fall Meeting 2005, abs. #OS22A–07.

Reves-Sohn, R., Humphris, S., and Canales, J.P., 2004, Cruise report: Seismicity and fluid flow of the TAG Hydrothermal Mound-4: Woods Hole, Massachusetts, Woods Hole Oceanographic Institution, ftp://obs.whoi.edu/pub/ras/STAG/STAG_Leg4_Cruise_Report.pdf (March 2007).

Rona, P.A., Pockalny, R.A., and Thompson, G., 1986, Geologic setting and heat transfer of black smokers at TAG hydrothermal field, Mid-Atlantic Ridge 26 degrees N: Eos (Transactions, American Geophysical Union), v. 67, p. 1021.

Rona, P.A., Hannington, M.D., Raman, C.V., Thompson, G., Tivey, M.K., Humphris, S.E., Lalou, C., and Petersen, S., 1993, Active and relict sea-floor hydrothermal mineralization at the TAG hydrothermal field, Mid-Atlantic Ridge: Economic Geology and the Bulletin of the Society of Economic Geologists, v. 88, p. 1987–2013.

Scott, R.B., Rona, P.A., McGregor, B.A., and Scott, M.R., 1974, The TAG hydrothermal field: Nature, v. 251, p. 301–302, doi: 10.1038/251301a0.

Smith, D.K., Cann, J.R., and Escartín, J., 2006, Widespread active detachment faulting and core complex formation near 13°N on the Mid-Atlantic Ridge: Nature, v. 442, p. 440–443, doi: 10.1038/nature04950.

Temple, D.G., Scott, R.B., and Rona, P.A., 1979, Geology of a submarine hydrothermal field, Mid-Atlantic Ridge, 26°N latitude: Journal of Geophysical Research, v. 84, p. 7453–7466.

Thompson, G., Mottl, M.J., and Rona, P.A., 1985, Morphology, mineralogy, and chemistry of hydrothermal deposits from the TAG area, 26°N Mid-Atlantic Ridge: Chemical Geology, v. 49, p. 243–257.

Tivey, M.A., Schouten, H., and Kleinrock, M.C., 2003, A near-bottom magnetic survey of the Mid-Atlantic Ridge axis at 26°N: Implications for the tectonic evolution of the TAG segment: Journal of Geophysical Research, v. 108, p. 2277, doi: 10.1029/2002JB001967.

Tucholke, B.E., and Lin, J., 1994, A geological model for the structure of ridge segments in slow spreading oceanic crust: Journal of Geophysical Research, v. 99, p. 11,937–11,958.

Wernicke, B., 1995, Low-angle normal faults and seismicity: A review: Journal of Geophysical Research, v. 100, p. 20,159–20,174, doi: 10.1029/95JB01911.

White, R.S., McKenzie, D., and O'Nions, R.K., 1992, Oceanic crustal thickness from seismic measurements and rare earth element inversions: Journal of Geophysical Research, v. 97, p. 19,683–19,715.

Wilcock, W.S.D., and Delaney, J.R., 1996, Mid-ocean ridge sulfide deposits: Evidence for heat extraction from magma chambers or cracking fronts?: Earth and Planetary Science Letters, v. 145, p. 49–64, doi: 10.1016/S0012–821X(96)00195–1.

Zonenshain, L.P., Kuz'min, M.I., Lisitsin, A.P., Bogdanov, Y.A., and Baranov, B.V., 1989, Tectonics of the Mid-Atlantic rift valley between the TAG and MARK areas (26–24° N); evidence for vertical tectonism: Tectonophysics, v. 159, p. 1–23, doi: 10.1016/0040–1951(89)90167–4.

Manuscript received 21 November 2006
Revised manuscript received 5 March 2007
Manuscript accepted 23 March 2007

Printed in USA

GSA Data Repository Item: 2007###

Data Repository Item For: Kinematics and geometry of active detachment faulting beneath the TAG hydrothermal field on the Mid-Atlantic Ridge

Brian J. deMartin[1*], Robert A. Reves-Sohn[2], Juan Pablo Canales[2], Susan E. Humphris[2]

[1]MIT/WHOI Joint Program in Oceanography, Cambridge, MA 02139, USA
[2]Woods Hole Oceanographic Institution, Woods Hole, MA 02543, USA

[*]Now at Brown University, Providence, RI 02912, USA

This file contains:

I. Sample seismograms and phase picks

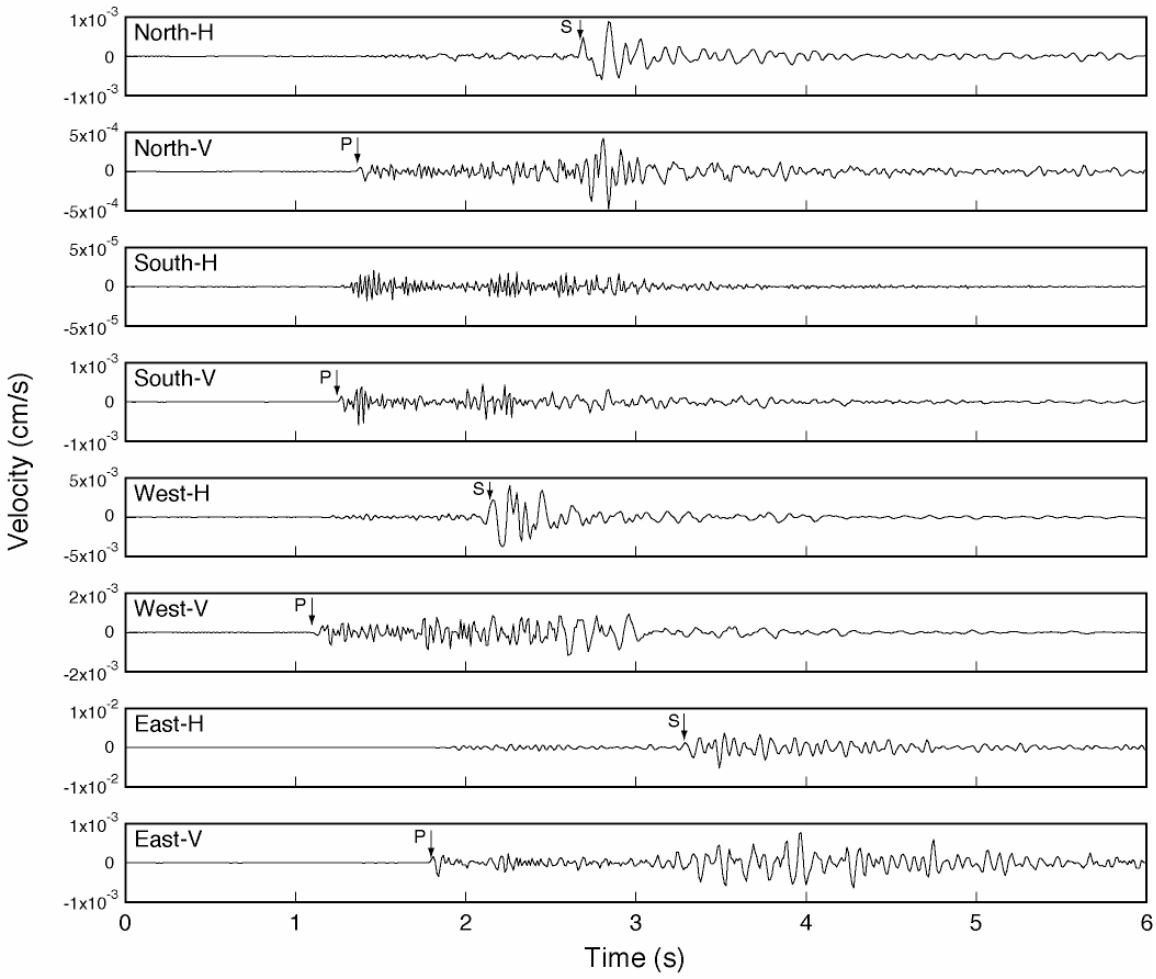

Figure DR1: Seismograms and compressional (*P*) and shear (*S*) phase picks from an event (M_L = 2.57) located on the detachment fault (at 26º 8.5'N, -44º 51.34'W, 6.5 km depth). Vertical (V) and horizontal (H) components of velocity are shown for the outermost ring of instruments in the network (i.e., North, South, East, and West instruments). Nominal arrival time uncertainties are 75 ms for *P*-waves and 150 ms for *S*-waves (note that no *S*-pick was made for the South instrument in this case). Data are band-pass filtered from 5-40 Hz.

II. Hypocenter catalog

P- and *S*- phase picks were made for 51,667 events detected by all 13 OBSs. Hypocenters were estimated via stochastic descent on a grid of rms residuals generated based on the difference between the phase picks and travel times predicted using William Menke's Raytrace3d program (Menke, 2005). Satisfactory hypocentral estimates (defined by rms residual < 0.12 s) were obtained for 19,232 events, with the rest being too far removed from the seismic network for accurate analysis. Hypocenter uncertainties were estimated at the 95% confidence interval using the method of Wilcock and Toomey (1991) as modified by Sohn et al. (1998). A hypocenter catalog in the format described in Table DR1 is available as a text file from the GSA Data Repository.

Table DR1. Sample entry from hypocenter catalog.

EQ Identification Number	Time*	Hypocenter rms residual (s)	Longitude (º)	± X (km)	Latitude (º)	± Y (km)	Depth Below Sea Level (km)	± Z (km)	Moment (N m)
124210310	01/24/2004 21:03:10.11	0.0827	-44.84634	0.50	26.14168	0.75	7.250	0.75	1.899E+18

*Time string is in month/day/year hour:minute:second format.

References:

Menke, W., 2005, Case studies of seismic tomography and earthquake location in a regional context.

Sohn, R.A., Hildebrand, J.A., and Webb, S.C., 1998, Postrifting seismicity and a model for the 1993 diking event on the CoAxial segment, Juan de Fuca Ridge: J. Geophys. Res., v. 103, p. 9867-9877.

Wilcock, W.S.D., and Toomey, D.R., 1991, Estimating hypocentral uncertainties for marine microearthquake surveys: A comparison of the generalized inverse and grid search methods: Marine Geophysical Researches, v. 13, p. 161-171.

III. Composite focal plane solutions

Composite focal plane solutions provide a means to incorporate focal mechanism constraints from multiple events within a small area into a single focal plane estimate. The polarity (i.e., up or down) of the observed *P*- arrivals from a group of events is plotted on a single focal sphere, which reduces focal plane uncertainties provided the events share a common source mechanism. The composite mechanisms shown in Figure 1a were generated using *P*-wave polarity estimates from 3 sets of events; (1) 304 events on the arc of the detachment (depth interval of 4.4 to 9.0 km below sea level), (2) 543 events on the inboard (i.e., westernmost) linear trend of seismicity (depth interval of from 3.5 to 5.9 km below sea level), (3) 365 events on the outboard (i.e., easternmost) linear trend of seismicity (depth interval from 3 to 5.8 km below sea level).

IV. Active-source seismic data

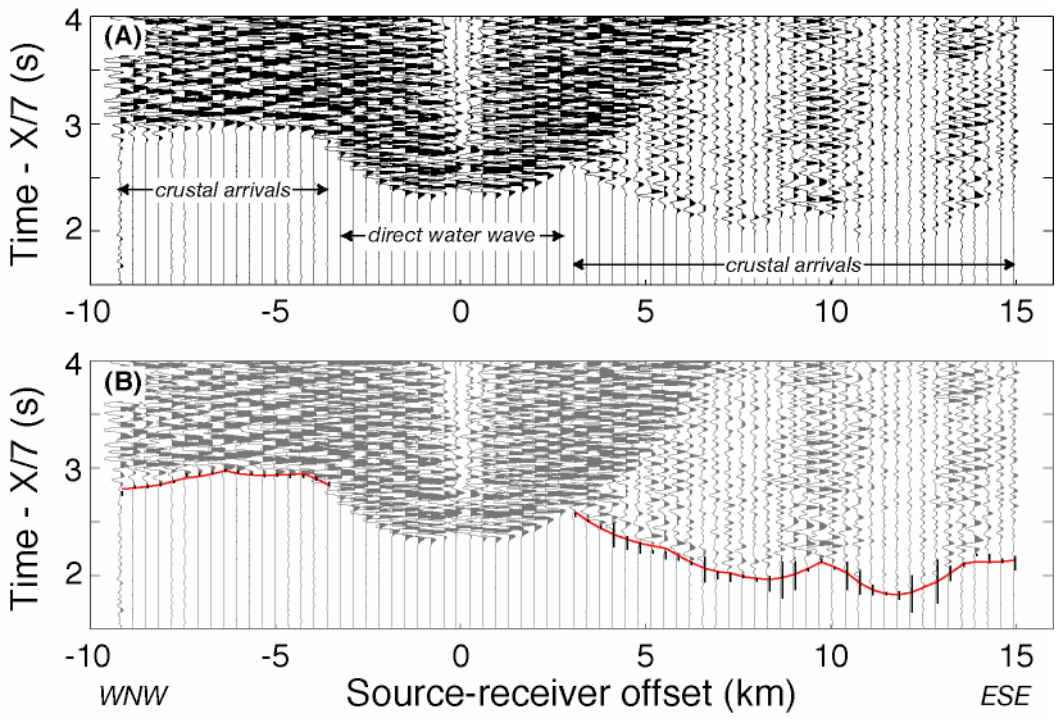

Figure DR2: (A) Example of active-source seismic record section for the OBS located 1 km to the west of the TAG mound. Vertical axis is travel time reduced to 7 km/s. Data have been band-pass filtered between 5 and 20 Hz, and amplitudes scaled according to range for display purposes. Labels indicate the nature of first arrivals at different offsets. Travel times were hand-picked, and uncertainty estimates included dependency on the signal-to-noise ratio, uncertainty in both source and receiver locations, and uncertainty in seafloor ray entry points due to out-of-plane topography. (B) Same as (A), with observed travel time picks (vertical bars with length equal to twice the assigned uncertainty) and predicted travel times (red line) by the preferred 2-D model shown in Figure 2a.

V. Tomographic resolution

We performed synthetic tests to determine the accuracy of inferring fault dip angles in the upper 3 km of the crust from the tomography model shown in Figure 2. We inverted synthetic travel times predicted by several models in which we imposed velocity anomalies resulting from extension and uplift along a fault, varying the fault dip, and then estimated the fault dip from the resulting tomography models. We found that our experiment can measure fault dips with an accuracy of ±5° if the fault dip is less than 35°. Faults dipping at steeper angles would be imaged in our tomography models with an apparent dip of 35°.

Additional tomography models along the axial valley of the TAG segment presented by Canales et al. (2005) show no evidence of low velocity zones beneath the TAG active mound. Resolution tests indicate that those tomographic inversions are capable of resolving low velocity anomalies beneath the TAG active mound with lateral dimensions ≥3 km if they are shallower than 4 km.